Supporting Information

Functionally active membrane proteins incorporated in mesostructured silica films

Justin P. Jahnke,[1] Matthew N. Idso,[1] Sunyia Hussain,[1] Matthias J.N. Junk,[1] Julia M. Fisher,[1] David D. Phan,[1] Songi Han,[1,2] Bradley F. Chmelka[1]*

[1] Department of Chemical Engineering and [2] Department of Chemistry and Biochemistry, University of California, Santa Barbara, California, 93106 United States

* To whom correspondence should be addressed: bradc@engineering.ucsb.edu

Contents

1. Protocols for expressing, purifying, and spin-labeling proteorhodopsin (PR) for incorporation into mesostructured silica films

The green-absorbing PR gene (BAC31A8), with the three natural cysteines mutated to serines, also with the additional photocycle-slowing E108Q mutation, was provided in a pTrcHis2 vector by E.F. DeLong and G. Whited, Genencor. The triple-cysteine mutant (TCM) is the most commonly studied PR variant, because it is less subject to oxidation than the true wild-type protein, and therefore has enhanced stability[1] and only minor functional differences.[2] The PR TCM is denoted here as "wild-type." Both wild-type PR and PR E108Q genes were subsequently cloned into the ampicillin-resistant pET22b vector (Novagen) using standard molecular biology techniques, which enable the addition of a 6X Histidine tag at the C-terminal end of the protein which facilitates protein purification via nickel chromatography. The cysteine point mutations (A174C and T177C) made for subsequent EPR investigations were introduced by modifying the PR E108Q template by site-directed-mutagenesis methods, such as those provided by the Quikchange kit (Stratagene, La Jolla, California).

PR was expressed by transformation of the PR-pET26b vector (or desired cysteine mutant) into *E. coli* strain BL21(DE3) competent cells. Individual bacterial colonies or glycerol stocks derived from transformants were used to inoculate a 10 mL culture of LB media containing 100 μg/mL ampicillin and allowed to grow overnight at 37˚C. Liter-scale batches were then grown from this starter culture, and overexpression of PR was induced by the addition of 1 mM isopropropyl-β-D-thiogalactopyranoside (IPTG) and 10 μM all-trans-retinal upon reaching a cell density with OD_{600} ~ 0.8. The pink-colored PR-expressing cells were then harvested by centrifugation after 4 h of growth at 37 ˚C.

The remainder of the purification procedure was carried out in a cold environment (4 ˚C) in solutions that contained a phosphate buffer (50 mM potassium phosphate, 150 mM KCl, pH 8.2). The cells were first resuspended in phosphate buffered solution with 20 mM $MgCl_2$ and 0.2 mg/ml lysozyme, incubated with shaking for 1 h, and then lysed by sonication. After a low-speed centrifugation step to remove unbroken cells (2000 g), membranes containing PR were obtained by ultracentrifugation (220,000 g). Membrane proteins were then solubilized overnight in phosphate buffered solution containing 2 wt% of the dodecyl-β-D-maltoside (DDM) surfactant. The unsolubilized membrane portions were pelleted by high-speed centrifugation (15,000 g), and the amount of PR was quantified by UV-visible spectroscopy, as established in the literature.[3,4] The PR was then incubated with an appropriate amount of Ni-NTA agarose His-tag affinity resin (Qiagen, MD) equilibrated with phosphate buffered solution containing 0.05 wt% DDM. After binding the PR, the resin was washed with at least 10 resin volumes of phosphate buffered solution with 0.05 wt% DDM and 25 mM imidazole.

The spin-labeling procedure of PR mutants A174C and T177C was carried out while PR was bound to the Ni-NTA resin and in greater than 15 mL of the phosphate buffered solution with 0.05 wt% DDM titrated to pH 7. A 5X molar excess of the nitroxide label (1-oxyl-2,2,5,5-

tetramethyl-Δ3-pyrroline-3-methyl) methanethiosulfonate (MTSL, Toronto Research Chemicals) was added from a 340 mM DMSO stock solution of MTSL and allowed to react overnight at 4 ˚C. After labeling, the sample was washed with 10 resin volumes of phosphate buffered solution with 0.05% DDM and 25 mM imidazole to remove unreacted MTSL.

For both spin-labeled and unlabeled PR, elution of the protein from the Ni-NTA resin was carried by removing as much buffered solution as possible from the resin and incubating with an elution buffer containing 450 mM imidazole and 0.1 wt% of the PR monomer-enriching 1,2-diheptanoyl-*s*,*n*-glycero-3-phosphocholine (diC_7PC, Avanti Polar Lipids) surfactant. Surfactant-associated MTSL and imidazole were removed by filtration with Sephadex gel desalting columns (GE Healthcare) equilibrated with 0.1 wt% diC_7PC in the phosphate buffered solution. The PR solutions obtained were then concentrated to ~100 μL volumes using centrifugal concentrators (10,000 MWCO; Millipore). The sample volume was increased to ~2.2 mL with phosphate buffered solution containing 2 wt% diC_7PC and then the sample was mix overnight to increase the population of monomeric PR. Size-exclusion fast protein chromatography (FPLC) carried out the next day as described in the main text, using the standard DDM buffer (0.05 wt% DDM) to elute the protein.

2. Blue-Native PAGE gel of DDM-solubilized monomeric and oligomeric proteorhodopsin isolated by size exclusion chromatography

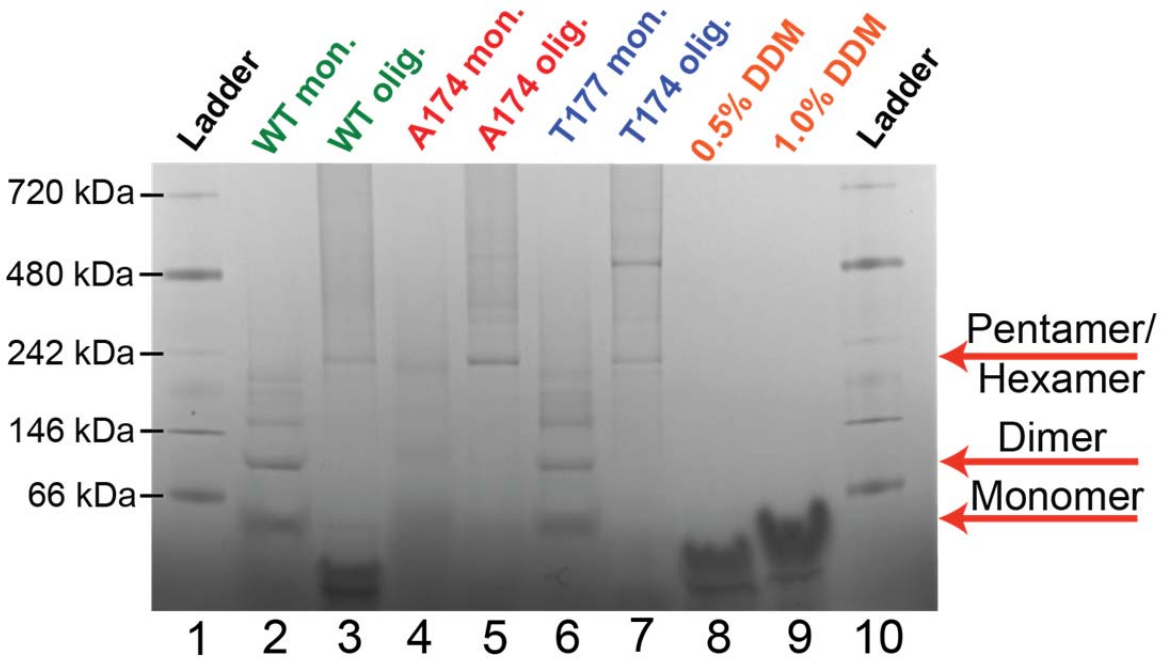

Figure S1. Blue-Native PAGE gel of wild-type (WT, well 2), A174R1-E108Q (well 4), and T177R1-E108Q (well 6) proteorhodopsin monomers isolated by size exclusion chromatography and exchanged non-buffered hydrochloric acid solutions (pH~4) with 0.05% DDM. Oligomeric proteorhodopsin in alkaline-buffered solutions (pH 9) collected from the same size-exclusion chromatography experiments are shown in wells 3, 5 and 7. The monomeric WT PR sample (well 2) show one intense band below the 66 kDa marker (well 1) and another below the 146 kDa marker (well 1) that are assignable to monomeric and dimeric proteorhodopsin species.[5] A number of lower intensity bands are observed above the 146 kDa marker (well 1) that presumably arise from oligomeric assemblies with more than two proteorhodopsin molecules. The wild-type proteorhodopsin oligomer sample (well 3) has a band at ~242 kDa that originates from pentameric/hexameric proteorhodopsin, while the two additional bands at molecular weights lower than that of monomeric proteorhodopsin likely arise from DDM micelles, as shown in wells 8 and 9. The monomeric and oligomeric fractions of both the spin-labeled A174R1-E108Q and T177R1-E108Q proteorhodopsin samples showed distributions similar to those of the wild-type proteins. Aqueous solutions (pH~7) with 0.5% and 1.0% DDM are shown in wells 8 and 9, respectively.

3. Images of DDM+diC$_7$PC-directed mesostructured silica films containing proteorhodopsin prepared with various compositions and synthesis conditions

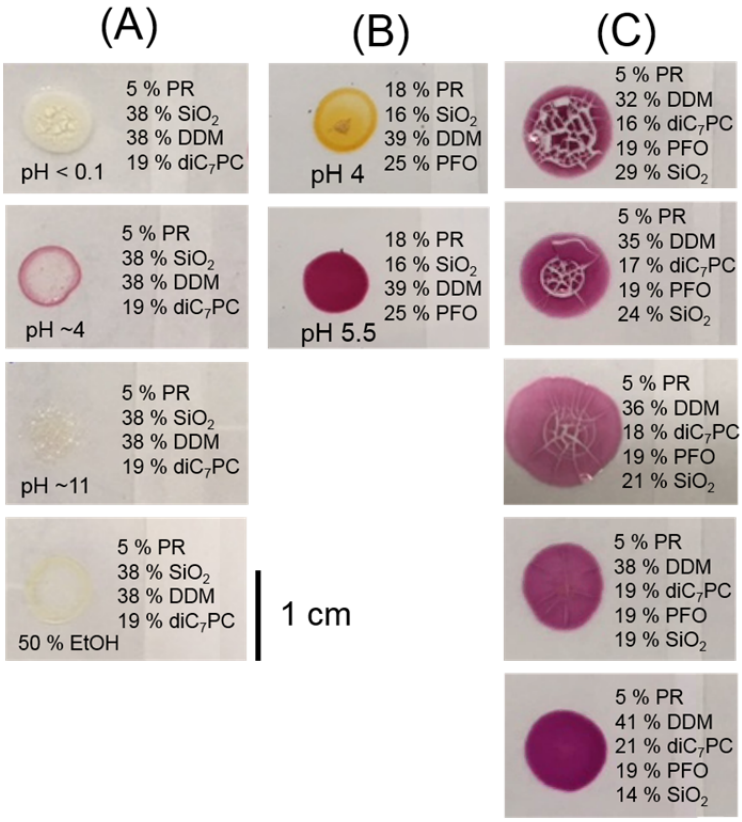

Figure S2. Macroscopic optical images of 50-100-μm-thick DDM+diC$_7$PC-directed silica films containing PR and cast on glass slides **(A)** without PFO under various pH and co-solvent conditions, **(B)** with PFO at either pH 4 or pH 5.5, and **(C)** using less water and with various silica contents. Mildly acidic (pH 4) synthesis conditions yielded films with purple colorations, consistent with functionally active PR. By comparison, films synthesized under conditions typical of conventional mesostructured silica materials, including at high acidities (pH <0.1), highly alkalinities (pH 11) or with 50% ethanol co-solvent, appeared yellow or transparent, indicative of denatured PR. As shown in (B), the anionic surfactant PFO promotes the formation of films with more homogeneous distributions of PR, though pH conditions higher than pH 4, such as at pH 5.5, are required to obtain films with functionally active PR. As the pI of PR is pH 5.8, PR is positively charged at pH 4 and therefore likely denatures in the presence of PFO as a result of strong attractive electrostatic interactions between PFO and PR, which are weaker at higher pH conditions. The macroscopic images in (C) reveal a lower propensity for macroscopic crack formation in silica films as SiO_2 content is decreased from 29 wt% to 14 wt%, which can be reduced by slowing the rate of drying.

4. N_2 sorption isotherm and BJH pore-distribution for DDM+diC_7PC-directed silica

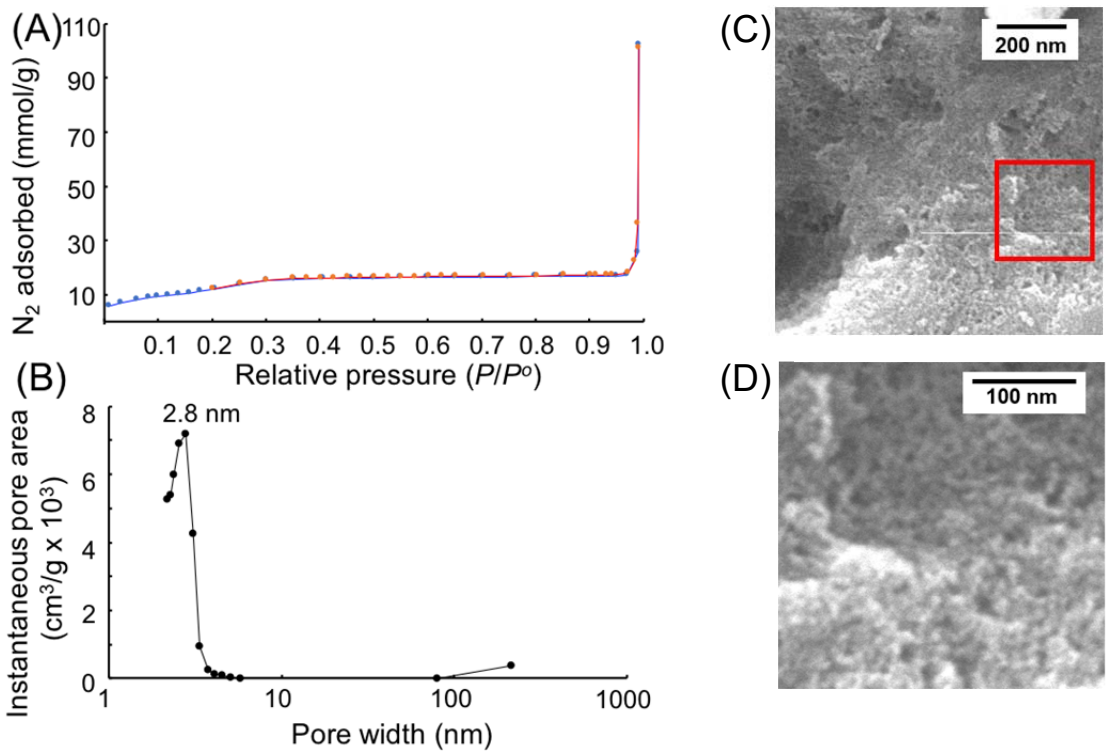

Figure S3. (A) N_2 adsorption (blue) and desorption (red) isotherms acquired from calcined DDM+diC_7PC-directed mesostructured silica materials synthesized with 40 wt% DDM, 20 wt% diC_7PC and 40 wt% SiO_2. The N_2 isotherm appears similar to a Type IV isotherm, but with a small hysteresis that indicates reversible capillary condensation and a substantial increase in N_2 adsorbed at the highest relative pressure. **(B)** Pore-size distribution calculated from the adsorption isotherm by using the BJH method, which exhibits a maximum ~2.8 nm, and a relatively narrow full-width-half maximum of 1 nm. This indicates a contraction of the framework as a result of calcination, with retention of relatively uniform mesopore dimensions. **(C, D)** Scanning electron microscopy images show a distribution of nanoscale textural features that are consistent with the BJH pore-size distribution and the small-angle X-ray scattering analyses for the as-synthesized material in Figure 2A.

5. Small-angle X-ray scattering patterns of mesostructured silica materials without and with proteorhodopsin guest species

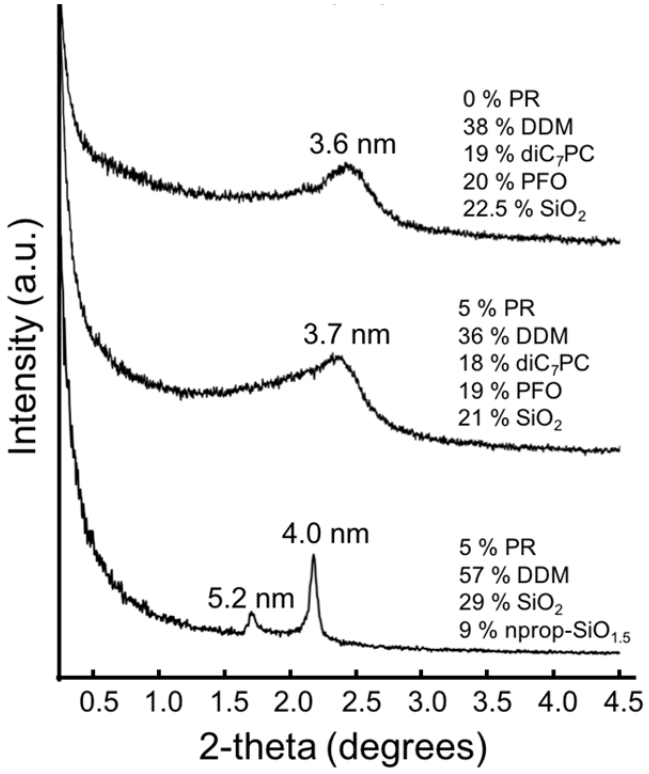

Figure S4. (A) Small-angle X-ray scattering (SAXS) patterns of mesostructured silica materials synthesized with various surfactant compositions: (**top**) 0 wt% PR, (**middle**) 5 wt% PR and (**bottom**) 5 wt% PR with low H_2O content during synthesis (H_2O ratio of 3.5:15), 29 wt% of SiO_2, and 9 wt% of *n*-propyl-$SiO_{1.5}$ organosilica.

6. Small-angle X-ray scattering patterns of DDM+diC$_7$PC-directed mesostructured silicas with different compositions of DDM and diC$_7$PC surfactants or calcined without PR

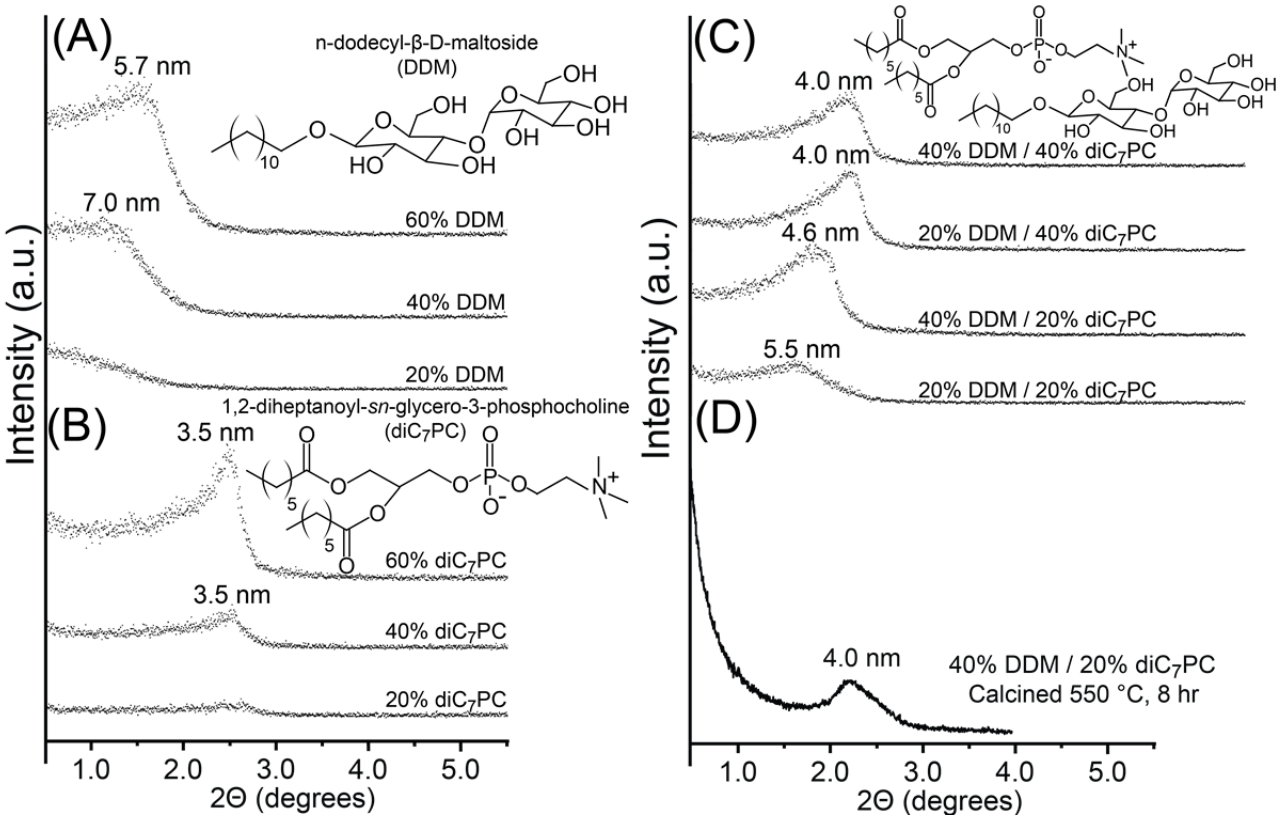

Figure S5. Small-angle X-ray scattering (SAXS) patterns of mesostructured silica materials synthesized using various quantities of **(A)** *n*-dodecyl-β-D-maltoside (DDM), **(B)** 1,2-diheptanoyl-*sn*-glycero-3-phosphocholine (diC$_7$PC), and **(C)** mixtures of DDM and diC$_7$PC as structure-directing surfactant species. Surfactant quantities are expressed as mass percentages of the final material (silica accounts for the balance), assuming complete solvent removal and silica cross-linking. Material precursor solutions were prepared by adding appropriate quantities of DDM and/or diC$_7$PC surfactants to aqueous solutions containing tetraethoxysilane silica precursor species, stirred under acidic conditions for 1.5 h. After the surfactants were dissolved, material solutions were titrated to pH 3-4 using 40 mM NaOH (aq.) and cast into Petri dishes under ambient conditions and allowed to dry for 2 days before SAXS characterization. **(D)** SAXS pattern of calcined mesostructured silica synthesized with 40% DDM, 20 % diC$_7$PC and 40% SiO_2, as described above, then calcined at 550 °C for 8 h; a single broad reflection is present at a *d*-spacing of 4.0 nm, consistent with contraction that occurs as a result of calcination of the as-synthesized material (*d*-spacing 4.6 nm, part C, 40% DDM and 20% diC$_7$PC).

7. Small-angle X-ray scattering patterns of DDM+diC_7PC-directed mesostructured silica with different loadings of proteorhodopsin (PR) species and PFO surfactants

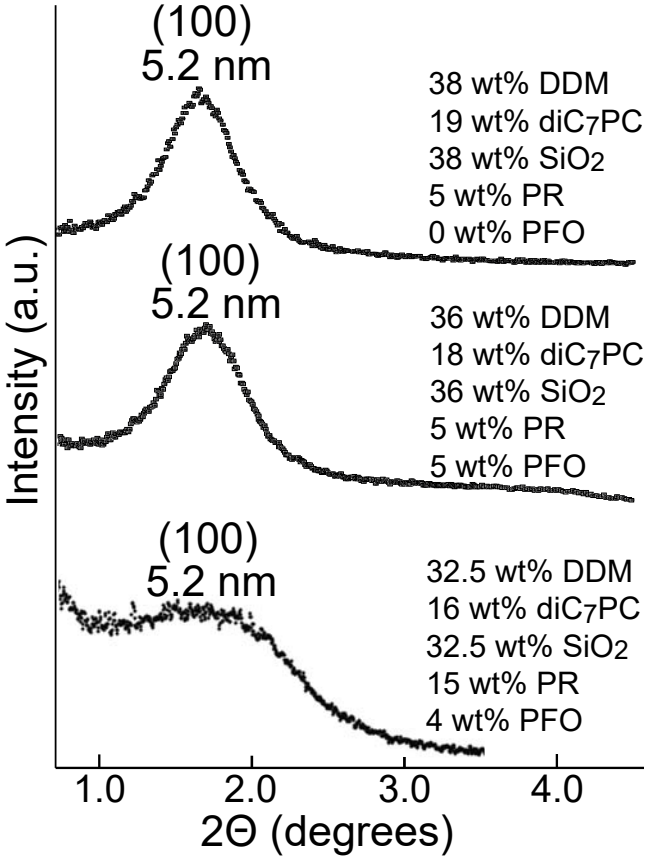

Figure S6. Small-angle X-ray scattering (SAXS) patterns of 50-μm thick DDM- and diC_7PC-directed mesostructured silica films with 5 wt% PR without (**top**) and with (**middle**) 5 wt% of PFO. The film that incorporates 5 wt% of PFO yields a primary *(100)* SAXS reflection at 1.7 ^{o} that is slightly broadened, yet otherwise identical to those of films without PFO, establishing the minor local effects of PFO molecules on the co-assembly interactions during formation of the silica-surfactant mesostructure. The SAXS reflection pattern (**bottom**) of a film that incorporates 15 wt% of PR has a primary *(100)* reflection position shifted to 1.7^{o}, corresponding to a 5.2 nm *d*-spacing, with a full-width-half-maximum of ~1.0 ^{o}.

8. Small-angle X-ray scattering patterns of P123-directed silica without and with DDM and 0.5 wt% proteorhodopsin

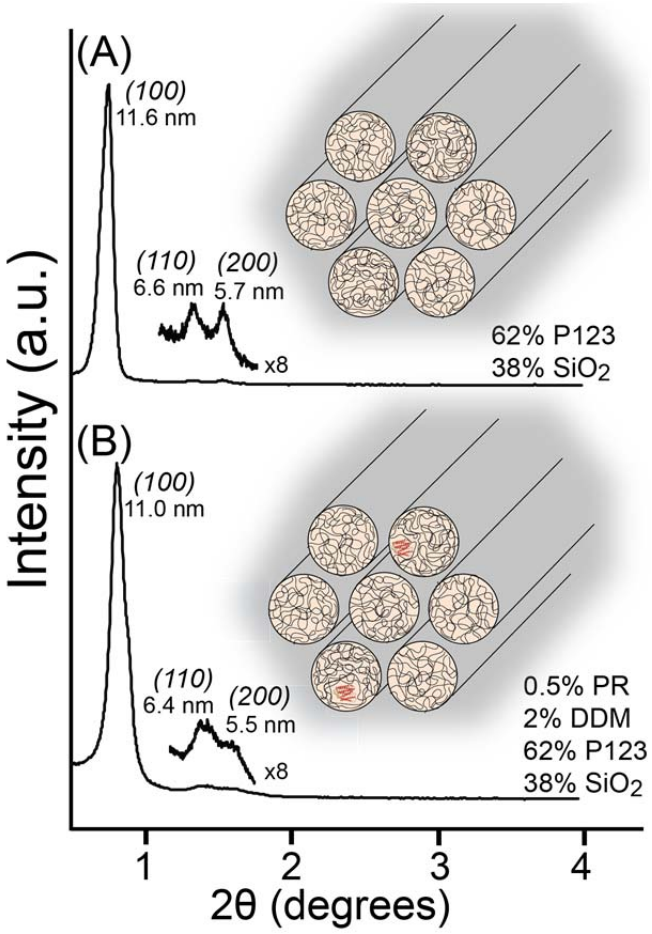

Figure S7. Small-angle X-ray scattering (SAXS) patterns from powders of P123-directed silica films **(A)** without and **(B)** with 0.5 wt% proteorhodopsin incorporated. Each pattern shows three reflections at ~0.8°, 1.3°, and 1.5° that are indexable to the (*100*), (*110*) and (*200*) reflections, respectively, associated with hexagonal (*p6mm)* mesostructural order. The patterns are similar, though with broader reflections observed in (B) for the film containing dilute PR and DDM, indicating reduced mesostructural order that diminishes further at higher PR loadings (not shown) and is accompanied by eventual loss of transparency of the films. Compared to conventional syntheses of P123-directed mesostructured silica, the somewhat lower extents of mesostructural ordering in these materials likely arises from the use of higher water contents, small quantities of DDM, and mild acidic conditions (pH ~4), which are necessary to stabilize PR molecules during co-assembly.

9. Table S1: Mechanical properties of mesostructured silica materials with 5 wt% PR

	Sample A		Sample B	
Region #	Hardness (MPa)	Modulus (MPa)	Hardness (MPa)	Modulus (MPa)
1	3.4	184	4.3	193
2	3.6	154	6.3	273
3	10.6	630	3.9	226
4	6.8	306	5.8	261
5	6.9	325	6.0	274
6	11.2	588	4.2	287
7	3.7	210	4.8	271
8	3.3	216	4.6	273
9	7.1	420	---	---
10	11.7	989	---	---
11	6.8	439	---	---
Average	6.8	406	5.0	257
St. deviation	3.0	239	0.9	29

Nano-indentation measurements were conducted to determine the hardness and modulus values of DDM+diC_7PC-directed mesostructured silica membranes containing 5 wt% proteorhodopsin guest species, without (Sample A) or with PFO (Sample B) synthesized on glass cover slips. The values for hardness and modulus reported in Table S1 were obtained using the Oliver-Parr method (which allowed for continuous measurement of hardness and modulus during loading) and represent the average hardness or modulus values obtained over the last 10% of the displacement. For each sample, several nano-indentation measurements were performed on different regions of the mesostructured silica membrane. Variations in the hardness and modulus values likely arise from heterogeneities in sample morphology and are more pronounced for Sample A, which exhibited a minor coffee-ring-like effect compared to Sample B, which was of more homogeneous. The composition of Sample A was 5 wt% PR, 38 wt% DDM, 19 wt% diC_7PC, 38 wt% SiO_2 and that of Sample B was 5 wt% PR, 36 wt% DDM, 18 wt% diC_7PC, 19 wt% PFO, 21 wt% SiO_2. These correspond to the materials for which SAXS and optical image results are presented in Figure 2B and 2C of the main manuscript.

10. Macroscopic images of cross-sections from mesostructured silica films with 5 wt% PR

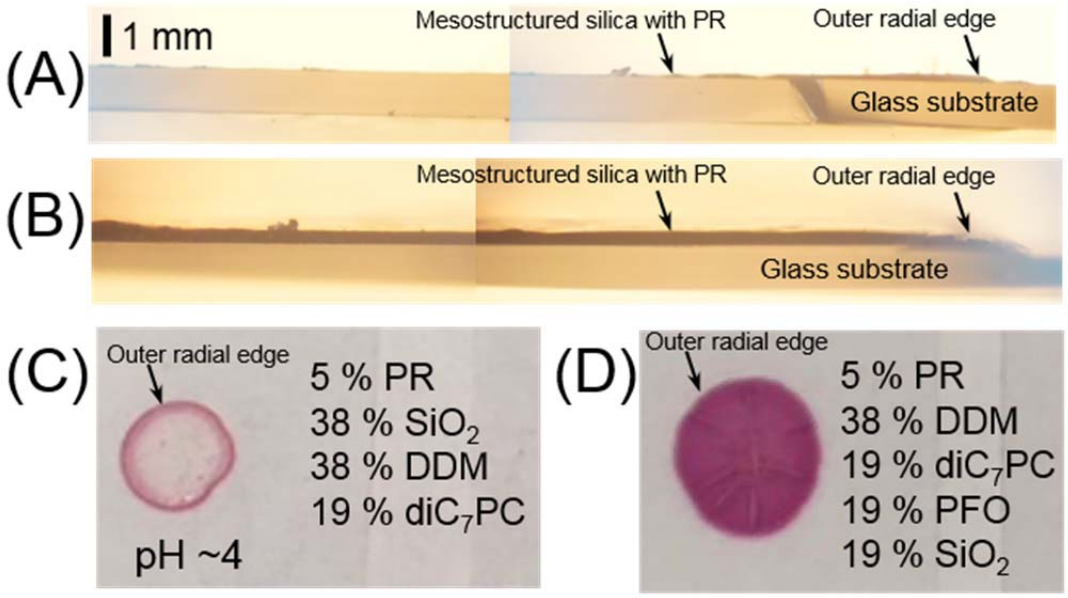

Figure S8. Macroscopic optical images of cross-sections from DDM+diC$_7$PC-directed mesostructured silica films synthesized with 5 wt% PR synthesized **(A)** without and **(B)** with 19 wt% PFO on glass substrates. The image in (A) was taken from **(C)** a film synthesized at pH 4 without PFO, which exhibits coffee-ring-like effects with the outer radial edge being thicker and darker than the center of the film. The image in (B) was taken from **(D)** a film with 19 wt% PFO, which yields a more homogeneous distribution of PR and thickness across the diameter of the film.

11. UV-visible absorption spectra of 20 wt% PFO mesostructured silica materials with and without PR

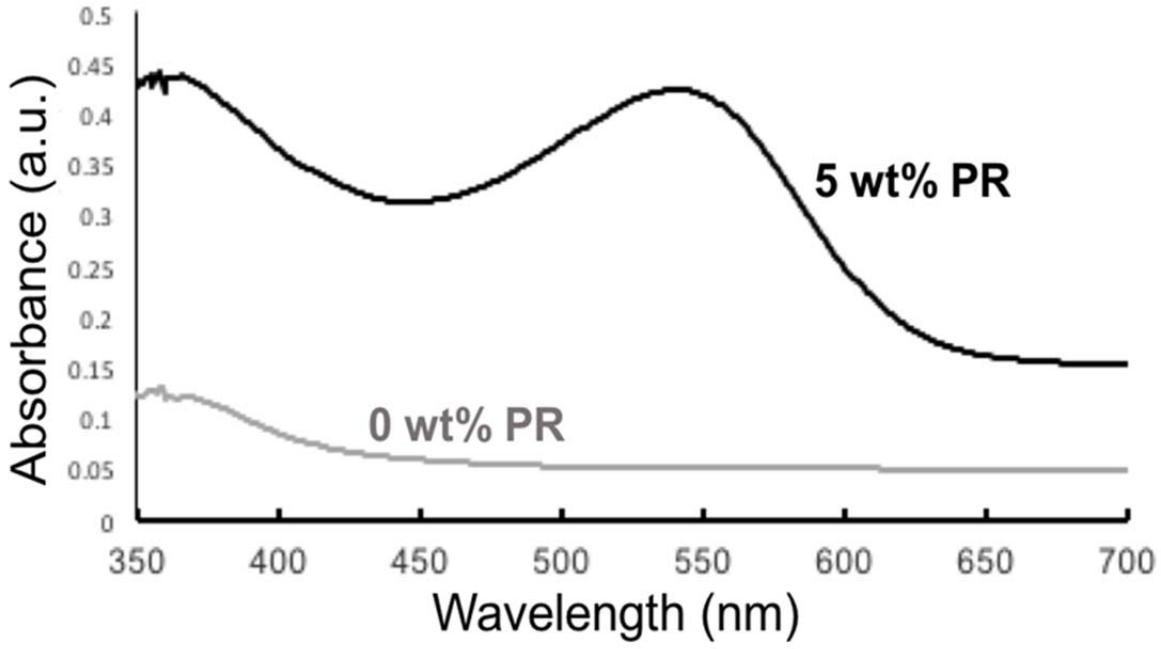

Figure S9. UV-visible absorption spectra acquired from DDM-diC_7PC+PFO-directed mesostructured silica films with either 0 wt% (grey) or 5 wt% (black) PR. The spectrum of materials without PR (grey) exhibits nearly constant and negligible absorbance over the visible range between 500 and 700 nm over which PR guests absorb. As neither film contains molecules that absorb at 700 nm, the greater absorption at 700 nm of films with PR (black) versus those without (grey) PR probably arises from differences in film thickness, morphology and/or alignment with incident light, rather than increased light scattering. The small absorbance centered at ~360 nm of films without PR (grey) likely originates from PFO molecules. The films were cast on borosilicate glass for both UV-visible absorption spectra shown here. These results indicate that the baseline background contribution can be considered to be minor in the absorbance spectrum for the otherwise identical DDM+diC_7PC+PFO-directed silica film containing 5 wt% PR.

12. Full 2D HYSCORE EPR spectrum of DDM-diC$_7$PC-directed mesostructured silica films containing 5 wt% PR

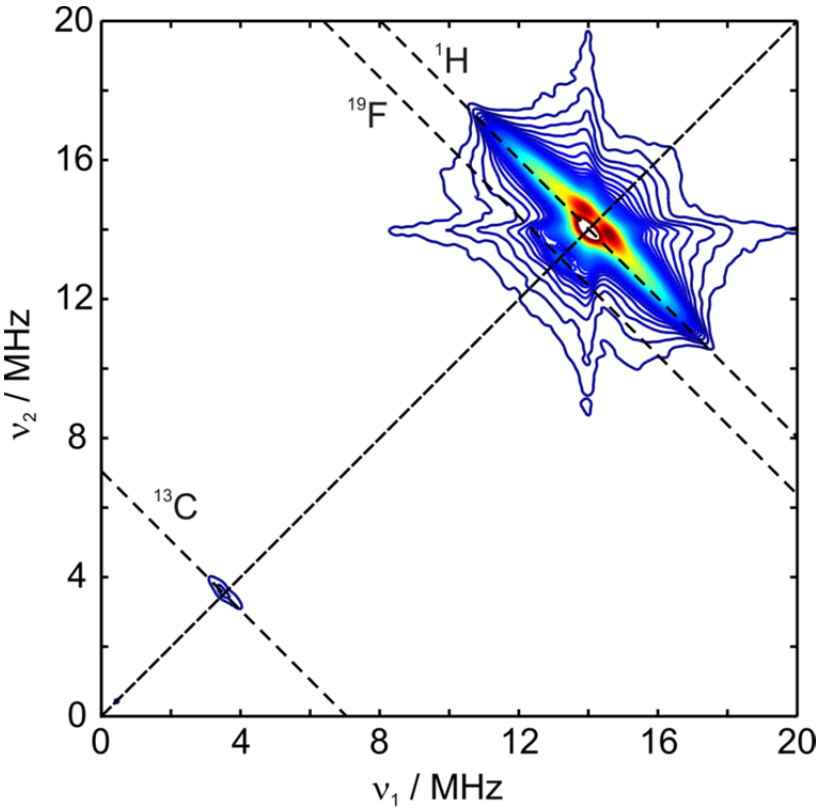

Figure S10. Full (+,+) quadrant of the HYSCORE EPR spectrum of a DDM+diC$_7$PC+PFO-directed silica film with 5 wt% proteorhodopsin labeled at the E-F loop residue 174 with the nitroxide spin label R1. The cumulative spectrum was obtained from two experiments recorded at 50 K with interpulse delays of 148 ns and 180 ns. Dashed anti-diagonals, which intersect the diagonal at 3.53 MHz, 13.19 MHz, and 14.02 MHz and correspond to the ^{13}C, ^{19}F, and ^{1}H Larmor frequencies at a magnetic field of 0.329 T, serve as guides to the eye. The lower cut-off value was decreased from 6% to 1.5% of the maximum signal intensity compared to the spectrum shown in Figure 4 of the main text. No appreciable signal intensity is observed in the (–,+) quadrant of the spectrum, which features signatures from strongly coupled nuclei with hyperfine couplings greater than their respective nuclear Larmor frequencies. Weak signal intensity at the ^{13}C Larmor frequency near the diagonal indicates weak coupling of the nitroxide spin to ^{13}C spins, which are present with a natural abundance of 1.1% in the protein and the surfactant.

13. $^{1}H\{^{19}F\}$ REDOR NMR spectrum of DDM+diC_7PC+PFO-directed mesostructured silica

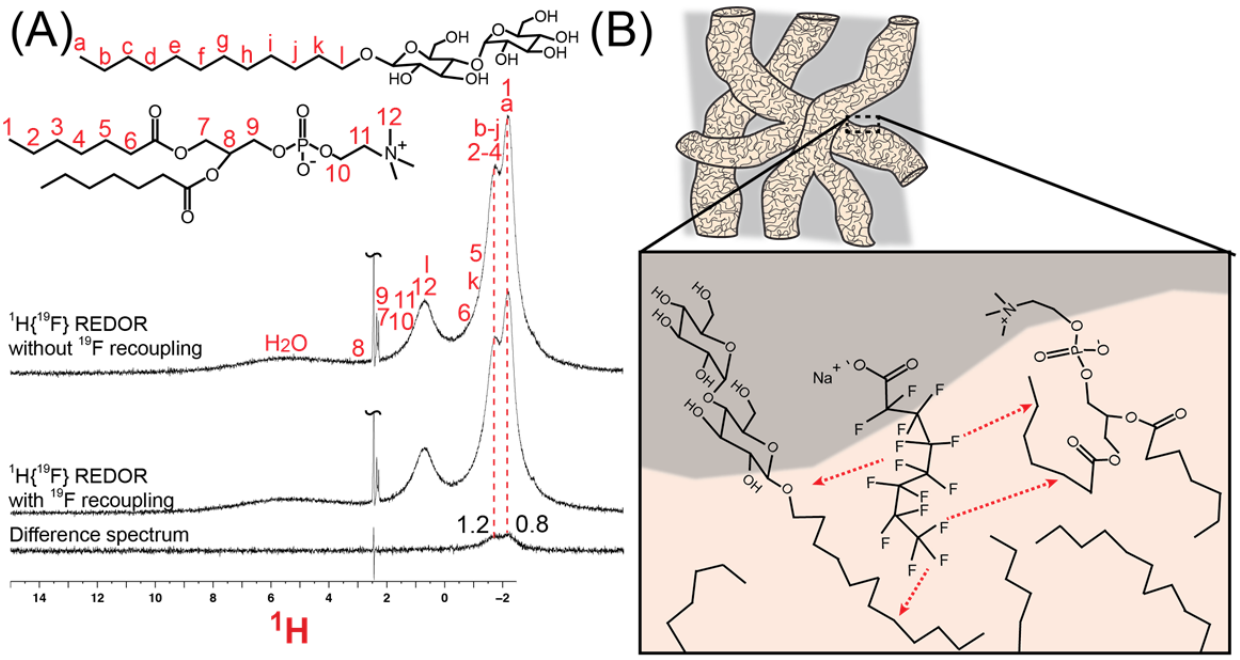

Figure S11. Solid-state $^{1}H\{^{19}F\}$ REDOR NMR spectra of DDM+diC_7PC+PFO-directed silica (5 wt% PFO), acquired without (**A, top**) and with (**A, middle**) reintroduction of ^{19}F-^{1}H dipolar couplings during a recoupling time of 0.11 ms, along with the corresponding difference spectrum (**A, bottom**). Signal intensities observed at 0.8 and 1.2 ppm (dotted red lines) are assignable to -CH_3 moieties *a* and *1* and -CH_2- moieties *b-j* and *2-4*, respectively, of the DDM and diC_7PC surfactant tails. As the only ^{19}F species in this material are associated with the PFO surfactant species, these signals establish the close proximities (<2 nm) of the PFO molecules to the structure-directing DDM and/or diC_7PC surfactants, as depicted schematically in (**B**). All spectra were acquired at MAS conditions of 15 kHz at approximately -20 °C.

14. Continuous-wave EPR spectra of P123-directed mesostructured silica materials containing PR with nitroxide spin labels at residues A174R1 or PR-T177R1

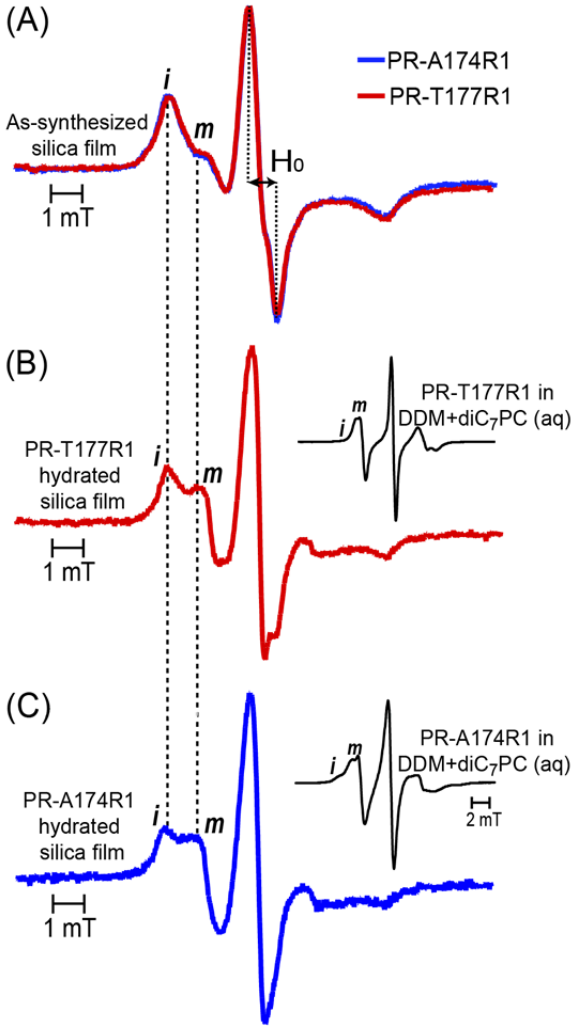

Figure S12. Continuous-wave EPR spectra of powders of P123-directed mesostructured silica films containing 0.5 wt% proteorhodopsin with nitroxide spin-labels at residues A174R1 or T177R1: **(A)** overlain spectra acquired from as-synthesized films, **(B,C)** spectra of films containing either (B) PR-T177R1 or (C) PR-A174R1 hydrated in alkaline-buffer (50 mM potassium phosphate, with 150 mM KCl, pH 9). The insets of (B) and (C) show the EPR spectra of the corresponding spin-labeled proteorhodopsin in alkaline-buffered DDM+diC$_7$PC micellar solutions under the same pH and buffer conditions. The as-synthesized P123-directed mesostructured materials with PR-A174R1 and PR-T177R1 have linewidths of 0.63-0.68 mT that are broader than the 0.23-0.31 mT linewidths of identically-labeled PR (Figure S6 B,C, insets) in alkaline-buffered DDM+diC$_7$PC micellar solutions. After hydrating the P123-directed mesostructured silicas in alkaline-buffered solutions, the EPR linewidths decrease by factors of 1.8 and 3.0 for materials that incorporate PR-A174R1 and PR-T177R1, respectively.

15. UV-visible absorption analyses of PR guest leaching from DDM+diC$_7$PC-silica materials upon exposure to alkaline buffered solutions

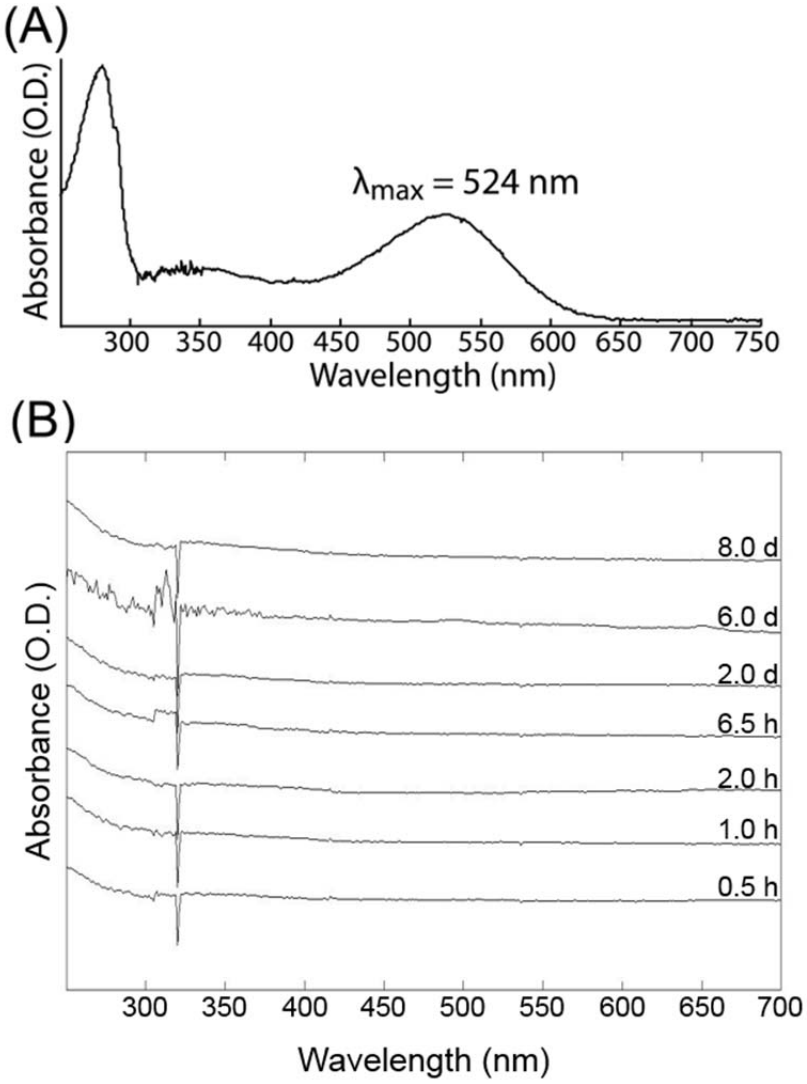

Figure S13. (A) Absorbance spectrum of PR in DDM micellar solutions under alkaline (pH~8.0) conditions. Two absorbance maxima are observed, one at 280 nm and another at 520 nm that arise largely from aromatic groups of the protein backbone and the retinal chromophore, respectively. **(B)** Absorbance of alkaline buffered solution with 0.5 wt% DDM that was mixed with DDM+diC$_7$PC-directed mesostructured silica materials that included 5 wt% wild-type PR at various amounts of times ranging from 0.5 h to 8 days from the initial exposure. No absorbance intensity is observed in the visible region near 520 nm or at 280 nm at any time, establishing that PR guests have not leached from the mesostructured silica materials. The positive absorbance at wavelengths below 300 nm may originate from scattering from in the sample or absorbance by the cuvette. Absorbance measurements in (B) were recorded on the supernatant solution obtained by centrifuging the material and solution mixture. The composition of mesostructured silica materials characterized in (B) was 28 wt% SiO_2, 60 wt% DDM, 7 wt% diC$_7$PC, and 5 wt% PR. Exposure of mesostructured silica materials with 16 wt% (or less) SiO_2 to aqueous solutions, however, resulted in partial leaching of PR guest species from the host materials.

16. Optical absorption difference spectra of 5 wt% PR (mutant E108Q) in an as-synthesized DDM+diC$_7$PC-directed mesostructured silica film and in *E. coli* membranes

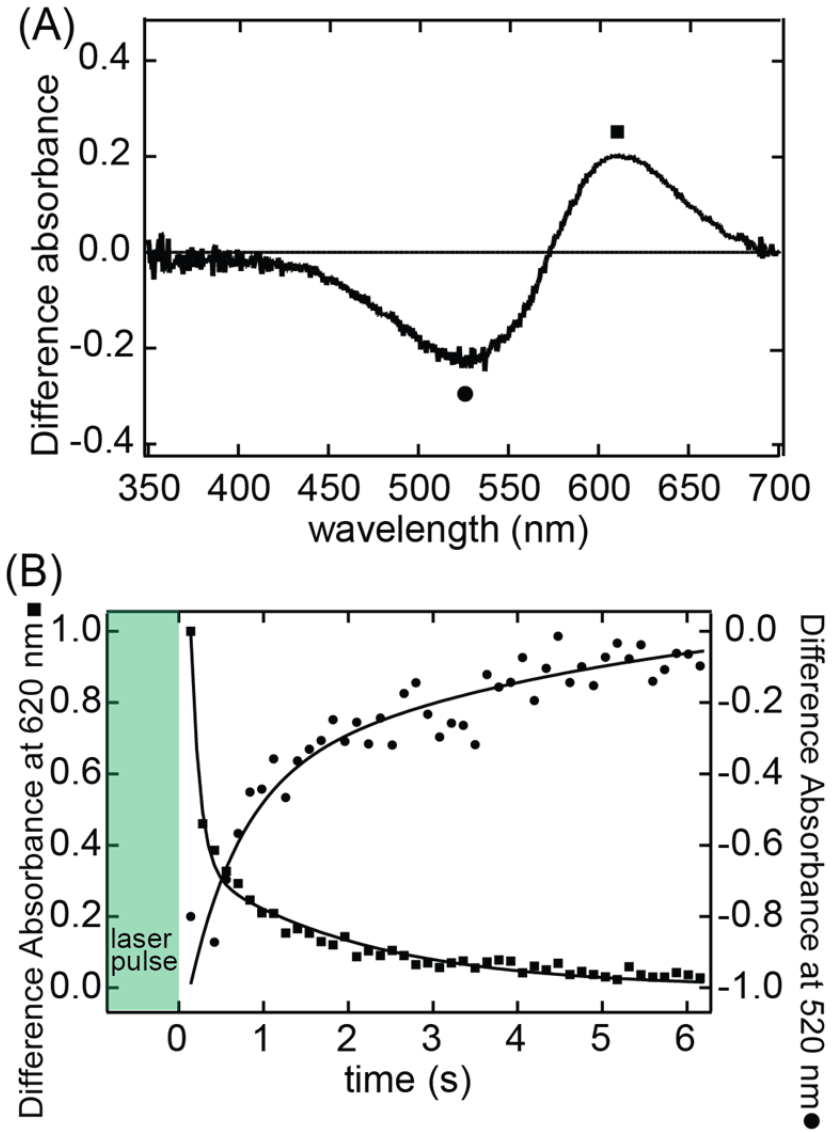

Figure S14. (A) Optical absorption difference spectra upon photo-activation of PR (slowed-photocycle E108Q mutant) spin-labeled with the nitroxide R1 at residue A174, incorporated at ~5 wt% in a DDM+diC$_7$PC-directed mesostructured silica film. The free-standing film was measured as-synthesized, without hydration or alkaline buffering. The spectrum shown was taken 130 ms after the sample was photo-activated with a 500 ms (~5 mW) green laser pulse. **(B)** Transient decay of the absorption amplitude at 620 nm (possibly a photo-intermediate in the later part of the PR photocycle stabilized by the DDM+diC$_7$PC-silica film), and intensity buildup at 520 nm (replenishment of the equilibrium PR state), are fit to biexponential curves.

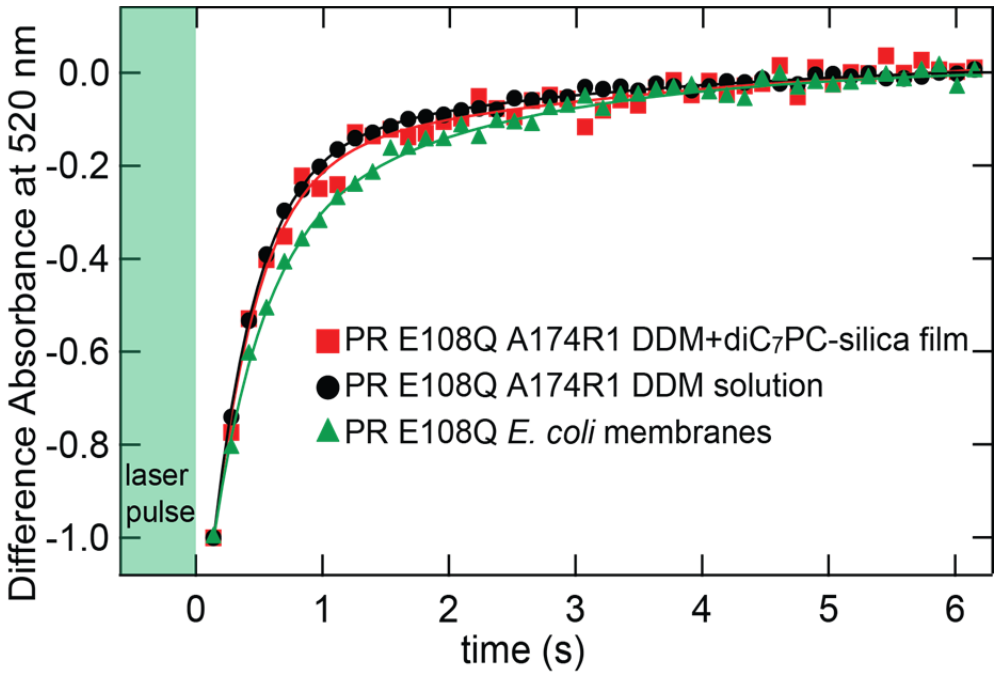

Figure S15. Time-resolved difference absorbance at 520 nm, following a green laser pulse, for PR in various environments: (1) in a DDM-diC$_7$PC-silica film hydrated with phosphate buffer (50 mM potassium phosphate, 150 mM KCl), (2) in a DDM micelle solution (0.05 wt% DDM in the same phosphate buffer), both shown in main text Figure 5, and (3) in extracted *E. coli* membranes resuspended in the phosphate buffer. All spectra were measured for mild alkaline conditions (pH 9) and fit to biexponential curves, which reveal that the PR E108Q photocycle displays similar characteristic time constants for the conditions tested. The increase in difference absorbance at 520 nm corresponds to the replenishment of the equilibrium *PR* state.

17. Continuous-wave EPR spectra of PR-A174R1 in DDM micellar solutions and P123-directed mesostructured silica with and without photo-activation

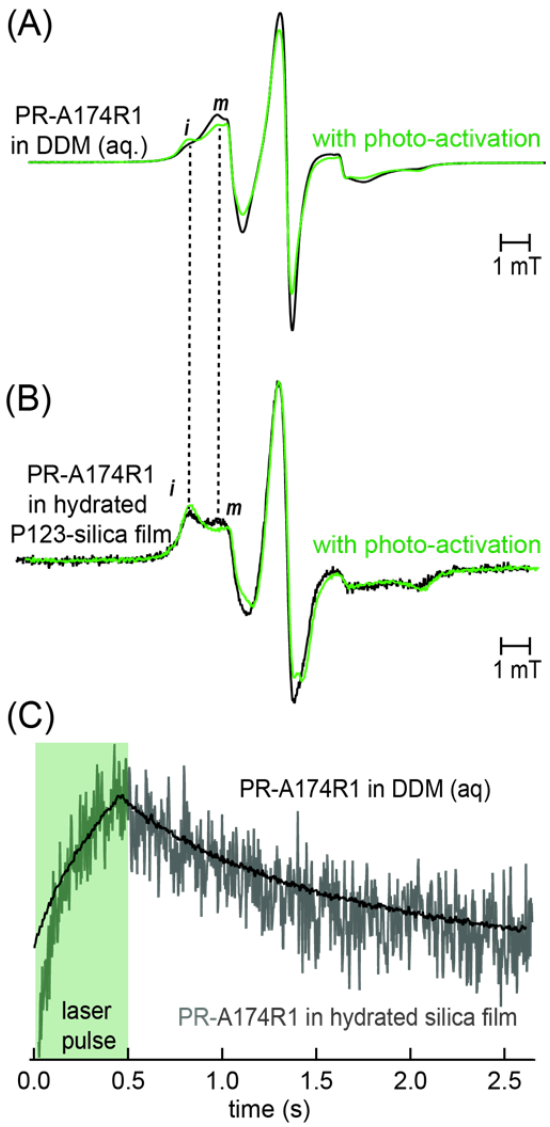

Figure S16. Continuous-wave EPR spectra (green) acquired under steady illumination by a green (532 nm) laser of the nitroxide spin-label (R1) attached to residue A174R1 of proteorhodopsin in **(A)** an alkaline (pH 9) buffered micellar solution (50 mM potassium phosphate, 150 mM KCl) of 0.05 wt% DDM and **(B)** a free-standing P123-directed mesostructured silica film with 0.5 wt% PR hydrated under the same buffer conditions. The EPR spectra (black lines) were acquired under identical conditions for the same samples without photo-activation for comparison. **(C)** Transient EPR amplitudes at the frequency corresponding to the relatively immobile (*i*) component of the EPR spectra of PR-A174R1 in hydrated P123-directed mesostructured silica films (grey line) and in the alkaline-buffered (pH 9) DDM+diC_7PC micellar solution (black line), directly following illumination of these samples with a green laser (~5 mW) pulse for 500 ms.

18. Supporting References

(1) Dioumaev, A. K.; Wang, J. M.; Bálint, Z.; Váró, G.; Lanyi, J. K. *Biochemistry* **2003**, *42*, 6582.

(2) Krebs, R. A.; Alexiev, U.; Partha, R.; DeVita, A. M.; Braiman, M. S. *BMC Physiol.* **2002**, *2*, 1.

(3) Lenz, M. O.; Huber, R.; Schmidt, B.; Gilch, P.; Kalmbach, R.; Engelhard, M.; Wachtveitl, J. *Biophys. J.* **2006**, *91*, 255.

(4) Friedrich, T.; Geibel, S.; Kalmbach, R.; Chizhov, I.; Ataka, K.; Heberle, J.; Engelhard, M.; Bamberg, E. *J. Mol. Biol.* **2002**, *321*, 821.

(5) Maciejko, J.; Mehler, M.; Kaur, J.; Lieblein, T.; Morgner, N.; Ouari, O.; Tordo, P.; Becker-Baldus, J.; Glaubitz, C. *J. Am. Chem. Soc.* **2015**, *137*, 9032.